

Article

Granular Skeleton Optimisation and the Influence of the Cement Paste Content in Bio-Based Oyster Shell Mortar with 100% Aggregate Replacement

Ana Cláudia Pinto Dabés Guimarães^{1,2}, Olivier Nouailletas³, Céline Perlot^{2,3,4}  and David Grégoire^{1,3,4,*} 

¹ Laboratoire des Fluides Complexes et Leurs Réservoirs, UMR5150, Université de Pau et des Pays de l'Adour, E2S UPPA, CNRS, LFCR, 64600 Anglet, France; anadabes@gmail.com

² Laboratoire des Sciences Pour l'ingénieur Appliquées à la Mécanique et au Génie Électrique, Université de Pau et des Pays de l'Adour, E2S UPPA, SIAME, 64600 Anglet, France; celine.perlot@univ-pau.fr

³ Institut Supérieur Aquitain du Bâtiment et des Travaux Publics, Université de Pau et des Pays de l'Adour, E2S UPPA, ISA BTP, 64600 Anglet, France; olivier.nouailletas@univ-pau.fr

⁴ Institut Universitaire de France, 75005 Paris, France

* Correspondence: david.gregoire@univ-pau.fr

Abstract: The purpose of this paper is to propose a methodology to optimise the granular skeleton assembly of cementitious materials containing non-spherical aggregates. The method is general and can be applied to any granular skeleton whatever the aggregate shape, size, or composition because it is simply based on the direct minimisation of the intergranular porosity to consequently increase the skeleton's compactness. Based on an experimental design approach, this method was applied to and validated for bio-based oyster shell (OS) mortar with 100% aggregate replacement. First, the best combination of seven crushed oyster shell particle classes was determined and compared with a standardised sand skeleton (0/4 mm) and three other non-optimised OS gradings in terms of intergranular porosity. In particular, it is shown that simply mimicking a reference grading curve initially designed for spherical particles with non-spherical particles led to poor performances. Then, different mortars were cast with the standardised sand skeleton, the optimised OS grading, and the three other non-optimised OS gradings by keeping the water-to-cement ratio (0.5), the aggregate bulk volume, and the cement paste content constant. Mechanical tests in compression confirmed the higher performance of the optimised OS mortar, validating the global optimisation approach. However, the high elongation of the oyster shell aggregates led to high skeleton intergranular porosities—even after optimisation—and the cement paste content needed to be adapted. For a given granular skeleton and for a constant aggregate bulk volume, the increase of the cement paste content led to an increase of both the filling ratio and the mechanical properties (compressive and flexural strengths). Finally, it is shown that the proposed skeleton optimisation and a cement paste content adjustment allowed recovering good mechanical properties for an oyster shell mortar with 100% aggregate replacement, especially in flexural tension.



Citation: Pinto Dabés Guimarães, A.C.; Nouailletas, O.; Perlot, C.; Grégoire, D. Granular Skeleton Optimisation and the Influence of the Cement Paste Content in Bio-Based Oyster Shell Mortar with 100% Aggregate Replacement. *Sustainability* **2024**, *16*, 2297. <https://doi.org/10.3390/su16062297>

Academic Editor: Seungjun Roh

Received: 22 December 2023

Revised: 28 February 2024

Accepted: 7 March 2024

Published: 10 March 2024

Keywords: bio-based materials; by-product valorisation; oyster shell; granular skeleton optimisation; full aggregate replacement; cement paste content



Copyright: © 2024 by the authors. Licensee MDPI, Basel, Switzerland. This article is an open access article distributed under the terms and conditions of the Creative Commons Attribution (CC BY) license (<https://creativecommons.org/licenses/by/4.0/>).

1. Introduction

Sustainability in construction and building materials involves various aspects, including raw materials, durability, and life cycle assessment. Concrete is a widely used material that is in high demand worldwide. However, the production of raw materials for concrete, including cement and aggregates, has numerous environmental impacts, such as climate change and resource depletion. To design more sustainable concrete, we can reduce the amount of traditional cement in the mix, use clinker-free cement, or replace extracted aggregate with recycled industrial waste. In particular, the construction industry has shown

an interest in the circular economy concept by using wastes as by-products in concrete. In addition, combining the natural properties of bio-based materials with conventional construction materials can enhance environmental quality and performance [1,2]. It is, therefore, logical to recycle and use industrial biological wastes in cementitious material. Crushed seashell waste is a great option because commercial mollusc farming is a vital part of the global aquaculture industry, accounting for 23% of the world's total production [3]. These farms produce a large amount of waste, with up to 90% of the mollusc's weight being represented by its shell [4]. Additionally, some seashells exhibit unique and outstanding mechanical properties [5–7], which make them ideal for use.

According to Robert et al. [8], in the 2010s, Europe produced 800,000 tons of molluscs per year, with a turnover of EUR 1100 million. This led to 37,000 direct employments and accounted for 50% of global EU aquaculture production by weight and 30% of the value. The main farmed species are oysters, mussels, and clams. In 2010, France produced 194,000 tons of molluscs, comprising 59% oysters, *Crassostrea gigas* (113,000 tons), 39% mussels, and 2% other molluscs such as cockles, clams, the King scallop, and the flat oyster [8]. (In 2017, the World Register of Marine Species (WoRMS) renamed *Crassostrea gigas* to *Magallana gigas*, but this name change is still debated in the community (see, e.g., [9,10]). In this paper, we will keep the former nomenclature, *Crassostrea gigas*.) *Crassostrea gigas* oysters are widely cultivated in France, with the region of *Nouvelle-Aquitaine* being the largest contributor (33.6%). Oyster farming generates a significant amount of waste (dead or diseased oysters, cleaning of parks), along with that from food consumption. The careless disposal of oyster seashell waste may cause several environmental problems such as soil contamination and a strong odour due to the organic matter or the microbial decomposition of salts into gases (NH_3 and H_2S) [11].

Oyster shell (OS) by-products have been valued in different activities such as heavy metal removal (e.g., [12]), soil supplement in agriculture (e.g., [13]), bio-applications (e.g., [14,15]), or construction and building materials. Regarding construction and building materials, significant research has been conducted in the last few years on utilising OS by-products as a supplementary cementitious material, alkaline-activated material, or aggregate replacement, and several review papers have been published recently (e.g., [16–20]). Yang et al. [21,22] examined the mechanical properties and durability of concrete with up to 20% crushed OS replacing fine aggregate. Eo and Yi [23] presented several concrete mixtures in which they substituted crushed OS for fine aggregate (ranging from 0 to 50%) and coarse aggregate (ranging from 0 to 100%), while considering various water–cement ratios. The replacement of conventional aggregate was examined individually for both fine and coarse aggregates in these concrete mixtures. Kuo et al. [24] conducted an analysis on the replacement of sand with OS (ranging from 5% to 20%) to create controlled low-strength materials. Meanwhile, Wang et al. [25] suggested an OS mortar that incorporated fly ash, with different replacement rates of traditional fine aggregate (sand): 5%, 10%, 20%, and 30%. Liao et al. [26] conducted experiments where they used a mixture of natural river sand and crushed waste oyster shells with varying particle sizes as fine aggregates in the preparation of mortar. Their findings showed that, as the content of oyster shells increased, the compressive and flexural strengths of the mortar decreased. Bamigboye et al. [27] mixed river sand, *Senilia senilis* seashells, and granite in varying proportions in concrete. It was observed that, as the proportion of seashells in the mixture increased up to 20%, there was a significant reduction in the compressive strength. However, the results in terms of split tensile strength were relatively good. After conducting a short literature survey, it can be concluded that using crushed OS particles as full or partial aggregate replacement in cementitious materials poses a challenge. Crushed OS aggregates have elongated and angular shapes, which is different from conventional spherical aggregates. This irregular shape and flatness may cause difficulties in terms of granular skeleton packing, increasing the porosity, and ultimately, leading to a decrease in mechanical performance [26]. This is why previous studies examined small replacement rates, but full aggregate replacement, especially in mortar, remains limited in the literature. Different methods have been employed in the previous articles to partially substitute traditional aggregate

with OS by-products. Wang et al. [25] and Kuo et al. [24] replicated standard particle size distributions (ASTM C33 and C136), while Yang et al. [21,22] and Eo and Yi [23] used a 5 mm sieved crushed OS mixture without emphasising any particular OS granular skeleton packing strategy. However, in classical mortar and concrete, having a compact granular skeleton is important to improve the mechanical and durability properties [28,29].

Various particle-packing models have been developed for classical cementitious materials to predict their packing density and increase compactness. The most widely used approach for optimising spherical aggregate packing density is to follow an ideal grading curve [30,31], which was first proposed by Fuller and Thompson in 1907 [32] and later developed by different authors (e.g., [33]). This approach is considered a trustworthy method for achieving good concrete mixes with spherical aggregates and is widely used by European standards. The method assumes a continuous particle size distribution, which means that the voids left by larger particles are filled by smaller particles and so on. As the studies on this topic have progressed, researchers have been able to identify the structural and interaction effects that occur between particles. The main effects that have been observed are as follows [31,34]. *The loosening effect*: This occurs when a fine particle disturbs the packing of a coarse particle frame, causing it to become loosened. *The wall effect*: This happens when additional voids are created by a coarse particle among a frame of fine particles. *The filling effect*: This occurs when fine particles tend to fill smaller voids created among the coarse particles' frame. *The occupying effect*: This happens when coarse particles are placed in the bulk volume of fine particles. Based on these considerations, different theoretical packing models have been proposed (e.g., [35–37]). Additionally, computational models using the discrete element method have been developed, which can simulate particle packing in both 2D and 3D structures (e.g., [30]). These models are effective at estimating the particle packing density for spherical particles. However, replacing conventional aggregates with non-spherical by-products remains a challenge for these models, particularly when performed at high rates.

Limited studies have been conducted to develop models for predicting the packing density of a blend with non-spherical particles [34]. Non-spherical packing theories are usually based on the assumption that their packing system can be considered similar to a spherical one. Yu et al. [38,39] described an approach for a binary system where non-spherical particles are related to spherical particles through an equivalent packing diameter, allowing the prediction of mix porosity. Goltermann et al. [37] worked out the concept of the Eigen packing degree and proposed an equivalent packing diameter for a multi-component aggregate. However, the definition of such a diameter is not obvious for OS particles because their shape changes with the particle size and the OS particles can be considered as lamellar particles (resting horizontally) or as standing needles in the concrete. Due to this problem, it is necessary to find another way to optimise the granular packing without using the equivalent diameter theory.

In this context, this paper intends to fill different research gaps. (i) A new methodology is proposed to optimise the packing of non-spherical particles in a granular skeleton. This method is general and can be applied to any granular skeleton, regardless of the shape, size, or composition of the aggregate. The method is based on the direct minimisation of the intergranular porosity, which, in turn, increases the compactness of the skeleton. (ii) The impact on the mechanical performances of a 100% replacement rate in oyster seashell mortar was evaluated along with the influence of the cement paste content. (iii) The study addresses the advantage of the proposed strategy compared to replicating a standard grading curve designed for spherical particles.

2. Materials and Methods

2.1. A Universal Methodology for Non-Spherical Granular Skeleton Optimisation

As explained in the Introduction, classical particle packing models are not suitable for particles that deviate significantly from a spherical shape. Therefore, a new approach is proposed for optimising the granular skeleton of cementitious materials that contain

non-spherical aggregates. This approach is applied to optimise the particle packing of crushed oyster shells as a full granular replacement of sand in a cementitious mortar.

The proposed approach relies on the direct optimisation of the intergranular porosity through the experimental design. To achieve this, the various particles were sorted into different classes and combined in different proportions, starting from the coarsest particles to the finest ones, in order to maintain the filling effect principle. For each particle class and combination of classes, the intergranular porosity was determined experimentally by measuring the loose bulk density and the oven-dried density (see Equation (1)).

$$\Phi = \frac{\rho_{od} - \rho_b}{\rho_{od}}. \quad (1)$$

In Equation (1), Φ is the intergranular porosity (-), ρ_{od} is the oven-dried density, and ρ_b is the loose bulk density. The oven-dried density and the loose bulk density were experimentally estimated by following the European standards NF EN 1097-6 [40] and NF EN 1097-3 [41], respectively.

The global skeleton assembly was selected with the aim of reducing the intergranular porosity on a global level. To achieve this, a statistical software (*Minitab 17*[®]) was used. The mix design used was the simplex centroid, and to ensure statistical significance, replicates were conducted for the vertex, double blends, and centre point.

The proposed method is versatile and can be applied to any granular skeleton, regardless of its shape, size, or composition. Its basis lies in the direct minimisation of intergranular porosity (Φ), which, in turn, increases the skeleton's compactness ($C = 1 - \Phi$). However, implementing the experimental design procedure practically can lead to certain limitations and drawbacks. The primary limitation is that it can result in a significant amount of experimental measurements of intergranular porosity, especially if a vast number of initial particle classes need to be combined. To simplify the process and reduce the number of experimental measurements, particle classes were combined in ternary mixes of three from the coarser classes to the finer ones. This approach does not consider all possible combinations and may not result in achieving the absolute minimum intergranular porosity. Another limitation is that the different particles first need to be sorted in different granular classes (e.g., following the NF EN 933-1 standard [42]), which may require the use of sieves designed for spherical particles. While the European standards NF EN 933-3 [43] and NF EN 933-4 [44] define the shape index and flakiness index, they are only useful for particle sizes greater than 4 mm and are, therefore, not useful for mortar formulation.

In our methodology, for the sake of simplicity and to ensure that the proposed methodology can be replicated in any classical civil engineering laboratory, we decided to follow the NF EN 933-1 standard [42] for particle sieving. However, when this standard is applied to crushed oyster shell aggregates, the high elongation of the particles may lead to variability in the sieving. Nevertheless, the sieving was only used for the initial sampling, and particle size distribution curves, such as the one presented in Section 3.2, were not used in the optimisation process. Particle size distribution curves are only presented in this paper for illustration or comparison purposes.

Table 1 and Figure 1 present and illustrate the generic experimental mix design used for the optimisation of a combination of three particle classes (A, B, and C) by minimising the resulting intergranular porosity after the experimental measurement of the oven-dried density and the loose bulk density for the 15 combinations.

After each round of optimisation, the real intergranular porosity of the best ternary mix suggested by the procedure was experimentally measured for confirmation.

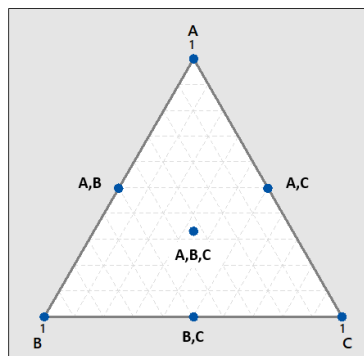


Figure 1. Illustration of the generic experimental mix design presented in Table 1.

Table 1. Generic experimental mix design used for the optimisation of a combination of three particle classes (A, B, and C) and illustrated in Figure 1.

Combination	Class Proportion		
	A	B	C
#1	1	0	0
#2	0	1	0
#3	0	0	1
#4	0.5	0.5	0
#5	0.5	0	0.5
#6	0	0.5	0.5
#7	0.33	0.33	0.33
#8	1	0	0
#9	0	1	0
#10	0	0	1
#11	0.5	0.5	0
#12	0.5	0	0.5
#13	0	0.5	0.5
#14	0.33	0.33	0.33
#15	0.33	0.33	0.33

2.2. *Crassostrea Gigas* Crushed Oyster Shell Material Description

The oyster shells (OSs) used in this study came from *Crassostrea gigas* grown in Arcachon Bay, France (see Figure 2). OSs are mainly composed of calcium carbonate CaCO_3 , with calcite as the dominant crystalline phase (see Figure 3). The farm cleaning process is the main source of production of OS waste, in addition to food consumption. After collection, OSs were stored in outdoor piles where they were naturally washed by rain. Finally, the OS aggregates were prepared through an industrial process consisting of hand collection of impurities, drying, crushing, and sieving into seven particle classes: 2.5/4 mm, 1.25/2.5 mm, 0.500/1.25 mm, 0.250/0.500 mm, 0.200/0.250 mm, 0.100/0.200 mm, and 0/0.100 mm.



Figure 2. Photograph of a *Crassostrea gigas* oyster shell from Arcachon Bay, France.

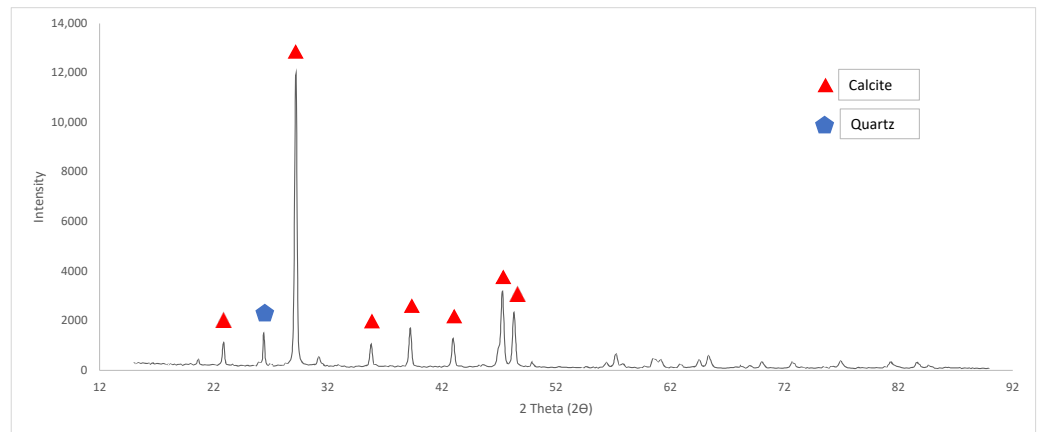


Figure 3. X-ray diffraction pattern of the *Crassostrea gigas* oyster shell.

2.3. Packing Optimisation of Crushed Oyster Shell Aggregates

The universal methodology for non-spherical granular skeleton optimisation presented in Section 2.1 was applied to the *Crassostrea gigas* crushed oyster shell (OS) aggregates presented in Section 2.2.

The particle groups were combined three by three in ternary mixes, and three rounds of optimisation were performed starting from the coarser classes to the finer ones. OSFA1, OSFA2, and OSFA3, respectively, denote the resulting mixes after rounds #1, #2, and #3 (see Figure 4). After the last round, the final optimised OS skeleton is denoted as OS1.

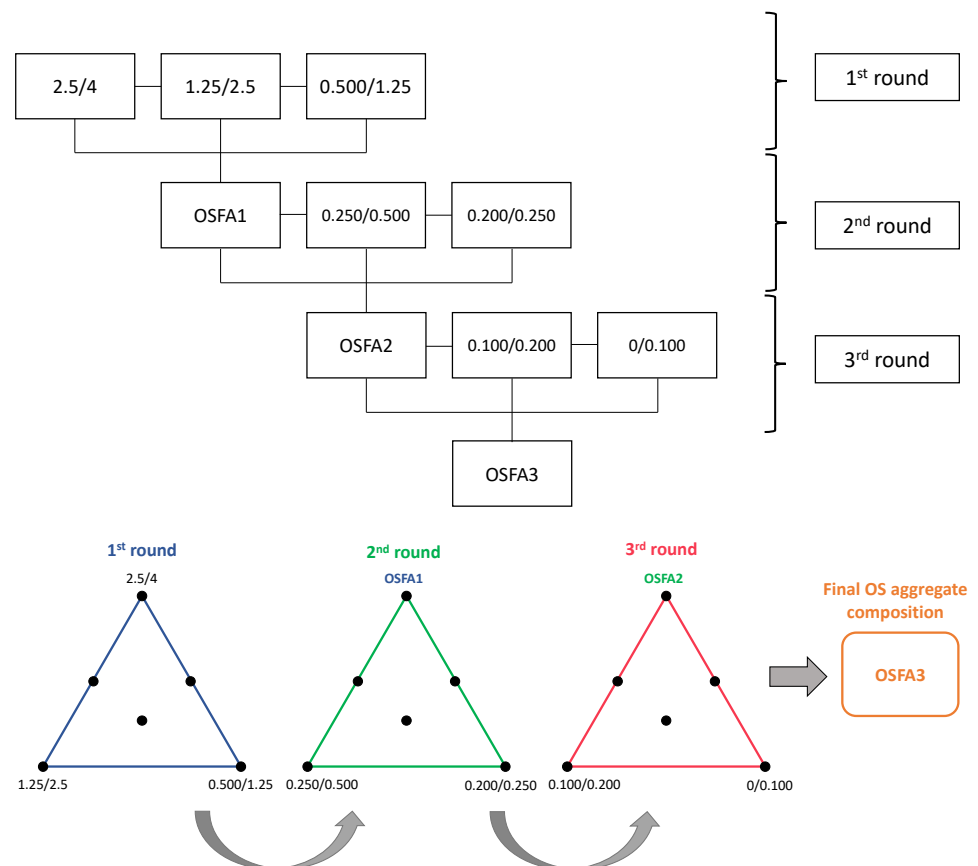


Figure 4. Principle of the optimisation of the oyster shell granular skeleton based on seven particle classes (2.5/4 mm, 1.25/2.5 mm, 0.500/1.25 mm, 0.250/0.500 mm, 0.200/0.250 mm, 0.100/0.200 mm, and 0/0.100 mm). OSFA1, OSFA2, and OSFA3, respectively, denote the resulting mixes after rounds #1, #2, and #3 of optimisation.

2.4. Mortar Material Description

An initial and reference mortar formulation, denoted as MS, was chosen following the European Standard NF EN 196-1 [45]. It incorporates a classical semi-crushed and washed sand 0/4 mm (siliceous alluvium), Portland cement CEMI 52.5N-PM-CP2 (97% clinker Portland and 3% secondary constituents, oven-dried density of 3180 kg/m^3), and water. The standardised proportions of water, cement, and sand aggregate are given in Table 2. The water-to-cement ratio is $W/C = 0.5$.

Table 2. Mix proportion of the initial and reference mortar incorporating a classical sand 0/4 mm.

Mortar	W/C	Water [kg]	Cement [kg]	Classical Sand (0/4 mm) [kg]
MS	0.50	0.225	0.450	1.350

Aggregates were fully replaced by volume in all oyster shell formulations. The oyster shell mortar based on the optimised granular skeleton (OS1) presented in Section 2.3 is denoted as MOS1. For comparisons, three other types of non-optimised oyster shell granular arrangements were designed with a constant range size (0/4 mm). OS2 denotes a mix designed with a higher amount of coarse particle classes. OS3 denotes a mix designed to mimic the classical sand grading curve. OS4 denotes a mix designed with a higher amount of fine particle classes. The corresponding grading curves are presented in Section 3.2, and the corresponding oyster shell mortars are denoted as MOS2, MOS3, and MOS4.

For the first batch of the five different mortars (MS and MOS1 to MOS4), the cement paste content was kept constant in addition to the aggregate volume and water-to-cement ratio. The corresponding formulations are given in Section 3.3. Then, two different MS mortars and three different MOS1 mortars were cast in a second batch with varying cement paste content, but with a constant aggregate volume and water-to-cement ratio. These mortars are denoted as MS_{*i*} or MOS1_{*j*}, where *i* and *j* are the percentage of voids of the given aggregated skeleton filled with the cement paste. The corresponding formulations are given in Section 3.4.

2.5. Mixing, Casting, and Testing Procedures

The mixing and casting procedures followed the European Standard NF EN 196-1 [45]. Due to the high water absorption coefficient (WA24) for OS mixes, all aggregate mixes were dried at $80 \text{ }^\circ\text{C}$ until reaching a constant mass and then stored in hermetic bags. From WA24, the water absorption content was estimated and the corresponding water amount was added to each bag 24 h before casting. The actual mixing procedure started by pouring the cement and the hydration water in a mixing bowl and then mixing at low speed for 30 s. Then, the aggregate was added steadily for 30 s, and the mixer was switched to high speed for an additional 30 s. Finally, the mixer was stopped for 90 s, then the mortar adhering to the wall was scrapped, and the mixer was restarted for an additional 60 s on high speed.

Beam samples of $40 \times 40 \times 160 \text{ mm}^3$ were cast, demoulded after 24 h, and immersed and cured in water at room temperature. After 7 or 28 days of curing, the different samples were mechanically tested in a saturated state on compressive or 3-point bending setups according to the European Standard NF EN 1015-11 [46]. Three replicates were tested for each formulation and each curing age.

The oven-dried density and the water absorption coefficient (WA24) were experimentally estimated by following the European standard NF EN 1097-6 [40] and the loose bulk density by following the European standard NF EN 1097-3 [41], and the intergranular porosity is given in Equation (1).

3. Results and Discussions

3.1. Validation of the Non-Spherical Granular Skeleton Optimisation Strategy Using Crushed Oyster Shell

Following the general methodology proposed in Section 2.1 and its application to crushed oyster shells (OSs) presented in Section 2.2, the seven OS particle classes (2.5/4 mm, 1.25/2.5 mm, 0.500/1.25 mm, 0.250/0.500 mm, 0.200/0.250 mm, 0.100/0.200 mm, and 0/0.100 mm) were combined three by three in ternary mixes, and three rounds of optimisation were performed to optimise the OS non-spherical granular skeleton. Figure 5 presents the extrapolated contour maps of the intergranular porosity obtained for the different ternary mixes for each round of optimisation by the statistical software *Minitab 17*[®] used in this study.

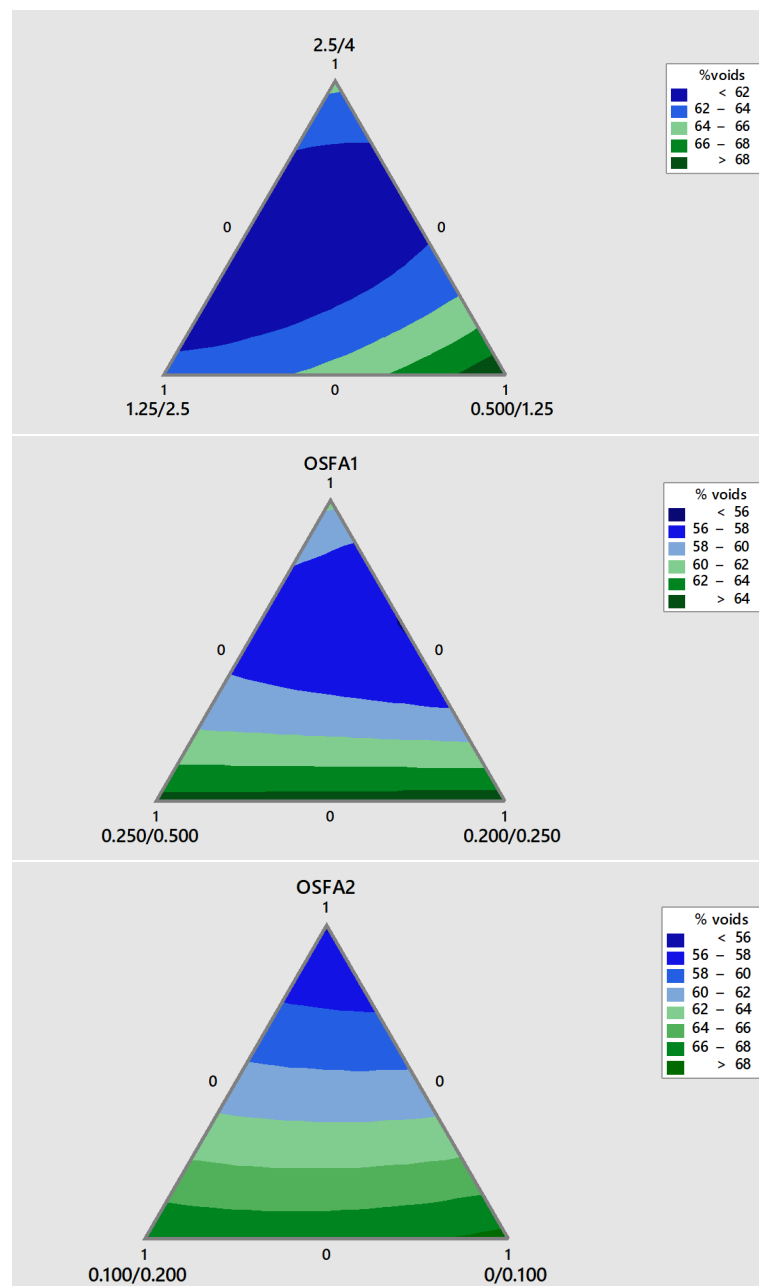


Figure 5. Extrapolated intergranular porosity for the different ternary mixes for each round of optimisation: **(top)** first round, **(middle)** second round, and **(bottom)** third round.

Figure 5 (top) shows that the best OSFA1 mix was a rather balanced combination of the three initial particle classes with an intergranular porosity lower than 62% (central dark blue region). In particular, the two green regions on the top- and bottom-right corners present an important intergranular porosity and should be avoided. More generally, any mix with a high proportion of 0.500/1.25 seems not to be favourable, with a clear tendency to increase the intergranular porosity when its proportion in the mix increases. The actual optimal OSFA1 mix was 37.4% of the 2.5/4 class, 44.5% of the 1.25/2.5 class, and 18.1% of the 0.5/1.25 class with a predicted intergranular porosity of 60.8%. An experimental measurement of 60.7% confirmed this prediction. Table 3 collects all predicted and experimentally measured intergranular porosities for each round of optimisation.

In the second round of optimisation, the next two particle classes (0.25/0.5 and 0.2/0.25) were combined together with OSFA1. Figure 5 (middle) shows that the best OSFA2 mix was a combination of the three particle classes where the intergranular porosity tended to be less than 58% (central blue region). Once again, the optimum intergranular porosity was obtained when combining the three particle classes in a rather balanced way. It is worth noticing that, starting from the central region, OSFA2's intergranular porosity increases with the increase of the 0.250/0.500 or 0.200/0.250 proportion, reaching a higher value than the initial OSFA1 one. This means that the initial OSFA1 mix may be highly disturbed by the addition of the smallest particles if they are not added wisely. The optimal OSFA2 combination was 58.6% of the OSFA1 class, 20.7% of the 0.25/0.5 class, and 20.7% of the 0.2/0.25 class with a predicted intergranular porosity of 56.7%. An experimental measurement of 56.3% confirmed this prediction.

In the third and last round of optimisation, the next two particle classes (0.1/0.2 and 0./0.1) were combined together with OSFA2. Figure 5 (bottom) shows that the best OSFA3 mix was a combination of the three particle classes, where the intergranular porosity tended to be less than 56% (top blue region). If a small amount of smaller particles may benefit to the final mix, Figure 5 (bottom) shows even more clearly than Figure 5 (middle) that the addition of smaller particles may highly disturb a given optimised mix if they are not added wisely, leading to intergranular porosity values that are higher than any individual ones obtained on a single particle class. This observation justifies why a specific methodology (as the one presented here) needs to be assessed for non-spherical granular skeleton optimisation. The optimal OSFA3 combination was 83.5% of OSFA2 class, 8.25% of the 0.1/0.2 class, and 8.25% of the 0./0.1 class with a predicted intergranular porosity of 56%. An experimental measurement of 54.1% was finally obtained for this mix.

The global strategy being validated by reaching a minima in terms of intergranular porosity, the optimised combination was now OS1, and it will be compared with other non-optimised oyster shell granular skeletons in Section 3.2. It is worth noting that we may not have reached the absolute minima in terms of intergranular porosity because some simplifications regarding the optimisation process were made by combining the particle classes three by three from the coarsest to the finest.

Table 3. Predicted and experimentally measured intergranular porosities for the best mix for every round of optimisation.

Round	Mix	Intergranular Porosity [%]	
		Predicted	Measured
#1	OSFA1	60.8	60.7
#2	OSFA2	56.6	56.3
#3	OSFA3	56.0	54.1

3.2. Comparison with Different Non-Optimised Oyster Shell Granular Skeletons

In this section, the optimised granular skeleton OS1, obtained in Section 3.1, is compared with that of a classical sand (S) and the three other non-optimised OS granular skeletons (OS2, OS3, and OS4) presented in Section 2.4. We remind the reader that OS2

denotes a mix designed with a higher amount of coarse particle classes, OS3 denotes a mix designed to mimic the classical sand grading curve, and OS4 denotes a mix designed with a higher amount of fine particle classes.

Figure 6 shows the particle size distribution of all granular arrangements. The classical sand S has a classical grading curve with a typical S-shape, and OS3's grading curve is perfectly superimposed. OS2 and OS4 have a typical grading curve of mixes, presenting a high amount of, respectively, coarse or fine particle classes. The optimised skeleton OS1 presents a particular grading curve with an "inverse" S-shape compared to the classical sand, the two curves crossing paths at around 0.5 mm.

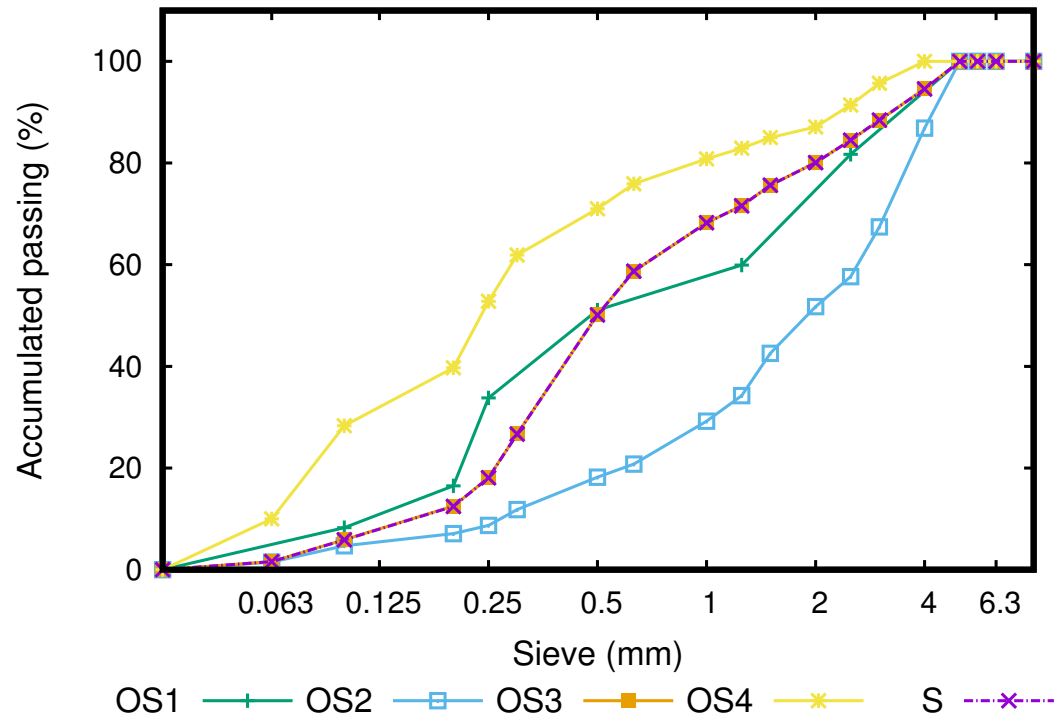
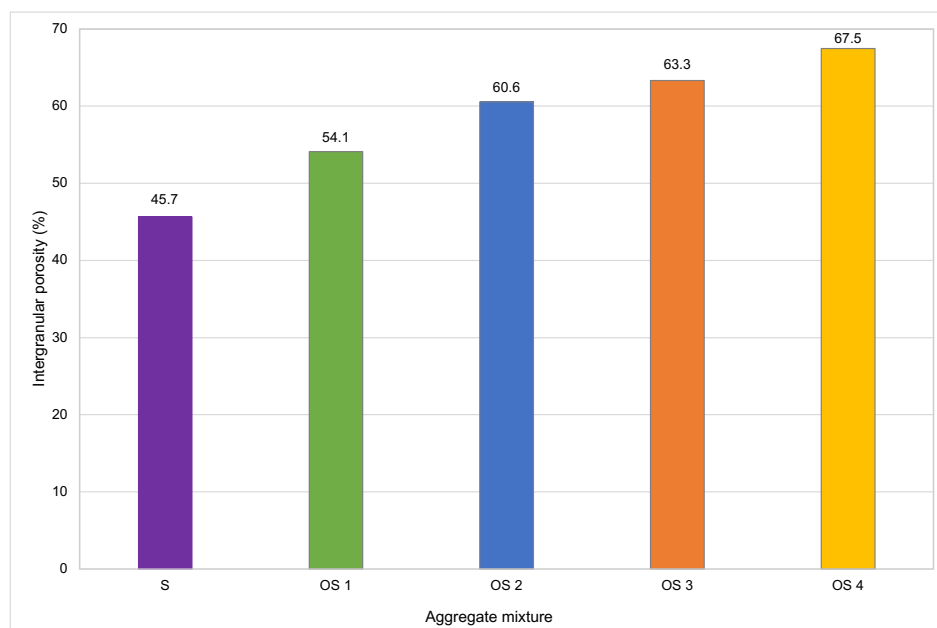


Figure 6. Particle size distribution of the different granular arrangements: classical sand S, optimised OS1, coarse OS2, sand-mimicking OS3, and fine OS4.

Table 4 presents the loose bulk and oven-dried densities for all aggregate mixes, and Figure 7 shows the corresponding intergranular porosity estimated through Equation (1). The oven-dried densities measured for the different OS skeletons were consistent with the results reported in the literature [21–24]. As expected, the reference sand skeleton, which was made of spherical particles, presented a lower intergranular porosity (45.6%). For the other non-spherical oyster shell aggregate mixes, the optimised OS1 presented the lowest intergranular porosity (54.1%), highlighting the efficiency of the optimisation method presented in Section 3.1. It is worth noticing that OS3, which mimics the classical sand arrangement, presented a very poor performance in terms of intergranular porosity (63.6%), especially when compared with OS2 (60.6%), which was not optimised, but designed with a high amount of coarse particles. Based on this result, we can recommend not mimicking spherical particle grading curves as non-spherical ones to minimise the resulting granular skeleton's intergranular porosity. The worse arrangement in terms of intergranular porosity was OS4 (67.5%), which was designed with a high amount of fine particles. This confirms the observation made in Section 3.1 that the addition of smaller particles may highly disturb a given mix if they are not added wisely. However, with a good optimisation methodology, as the one presented here, the smallest non-spherical particles may be assembled with the coarser ones to reach a low intergranular porosity (OS1) even if the absolute minima of a spherical arrangement (S) cannot be reached.

Table 4. Loose bulk density and oven-dried density of the different granular arrangements.

Skeleton	Loose Bulk Density [kg/m ³]	Oven-Dried Density [kg/m ³]
S	1462	2690
OS1	974	2123
OS2	852	2160
OS3	903	2463
OS4	840	2583

**Figure 7.** Intergranular porosity of the different granular arrangements: classical sand S (45.7%), optimised OS1 (54.1%), coarse OS2 (60.6%), sand-mimicking OS3 (63.3%), and fine OS4 (67.5%).

3.3. Compressive Performance of the Different Oyster Shell Mortars with 100% Aggregate Replacement and a Constant Cement Paste Content

The different crushed oyster shell (OS) skeletons presented in Section 3.2 were used as a 100% granular replacement of the classical sand in the standardised mortar formulation presented in Section 2.4. Aggregates were fully replaced by volume in all formulations, and the cement paste content was kept constant, in addition to the aggregate volume and water-to-cement ratio. Table 5 presents the water absorption coefficient (WA24) measured for the different granular skeletons S, OS1, OS2, OS3, and OS4. The values were consistent with the results reported in the literature [11,16,17,47]. The WA24 for OS aggregates was much higher than the one measured for classical sand, and this was taken into account in the mortar casting as developed in Section 2.5. Some authors [21,24] explain that the high amount of internal pores, the irregular aggregate surface, and the particle size can contribute to this increase of the WA24. We can indeed conclude from Figure 6 and Table 5 that the coarser is the granular arrangement, the higher is the WA24.

Table 5. Water absorption coefficient (WA24) of the different granular arrangements.

Skeleton	WA24 [%]
S	1.2
OS1	9.4
OS2	12.9
OS3	9.5
OS4	6.2

Table 6 presents the mix proportion for different mortar formulations at a constant cement paste content, constant bulk aggregate volume, and constant water-to-cement ratio.

Table 6. Mix proportion of the different mortar formulations at a constant cement paste content.

Formulation	A	W/C	Mass [kg]			Cement Paste Volume [m ³]	Aggregate Bulk Volume [m ³]
			W	C	A		
MS	S	0.50	225	450	1350	0.367	0.923
MOS1	OS1		225	450	899		
MOS2	OS2		225	450	786.3		
MOS3	OS3		225	450	833.5		
MOS4	OS4		225	450	755.3		

W: water, C: cement, A: aggregate, S: classical sand, OS1 to OS4: oyster shell granular skeletons.

Figure 8 presents the compressive strength evolution of all oyster shell mortar formulations after 7 days and 28 days of curing for a constant cement paste content. Usually, we observed an increase in the compressive strength from 7 to 28 days for all formulations with a relative increase of, respectively, 18%, 18%, 16%, and 8% for the MOS1, MOS2, MOS3, and MOS4 formulations. This increase was relatively small compared to the classical mortar (MS presented a relative increase of 30%), and the oyster shell may slow down the curing process. According to the intergranular porosity increase shown in Figure 7, the compressive strength decreased from MOS1 to MOS4, validating the global optimisation approach proposed here.

However, it is worth noticing that, for a constant cement paste content, a constant aggregate bulk volume, but different intergranular porosities, the same amount of voids was not equally filled in all OS mortar formulations. This will be studied in more detail in Section 3.4.

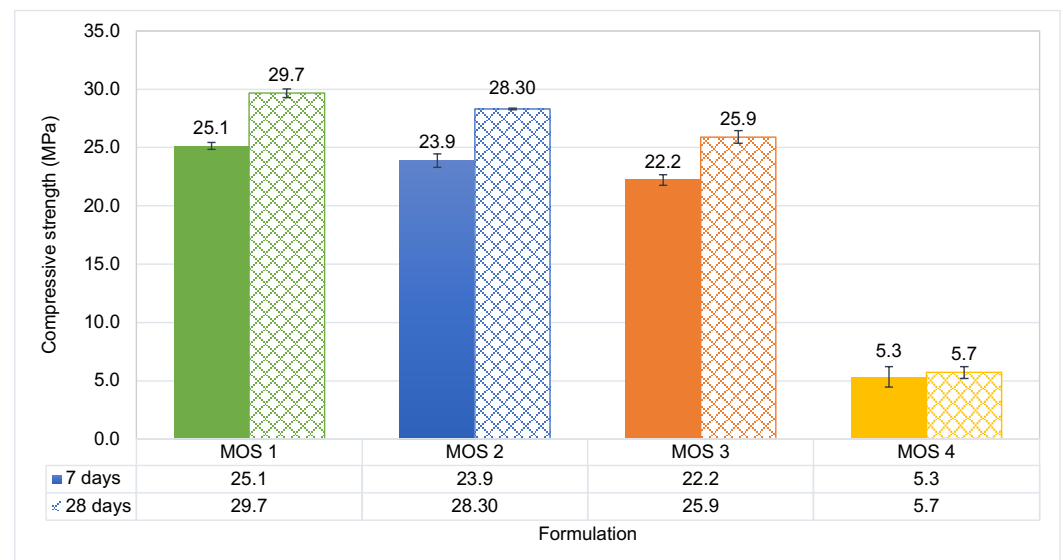


Figure 8. Compressive strength comparison of the oyster shell mortar formulations after 7 days (plain) and 28 days (cross-hatch) of curing at constant cement paste content. MS compressive strength: 45.4 ± 0.6 MPa at 7 days, 59 ± 2 MPa at 28 days.

3.4. Influence of the Cement Paste Content on the Compressive and Flexural Strengths

In this section, we study the influence of a varying cement paste content on the compressive and tensile mechanical properties of different mortars composed of a classical sand granular skeleton (S) or an optimised oyster shell granular skeleton (OS1). Two different MS mortars and three different MOS1 mortars were cast with varying cement paste content,

but with a constant aggregate volume and water-to-cement ratio. By varying the cement paste content, we varied the filling ratio, i.e., the amount of void filled with the cement paste. The different mortars are denoted as MS_{*i*} or MOS1_{*j*}, where *i* or *j* is the filling ratio. The corresponding formulations are given in Table 7. The filling ratio of the mortar formulations MS and MOS1 presented in Table 6 may be evaluated and were, respectively, 86.9% and 73.4%. These two mortars MS and MOS1 are then denoted as MS₈₇ and MOS₇₃. All formulations with varying filling ratios are given in Table 7.

Table 7. Mix proportion of the different mortar formulations with varying cement paste content.

Formulation	A	W/C	Mass [kg]			Cement Paste Volume [m ³]	Aggregate Bulk Volume [m ³]	Filling Ratio [%]
			W	C	A			
MS ₈₇ *	S	0.50	225	450	1350	0.367	0.923	86.9
MS ₁₀₀			258.5	516.9		0.421		99.9
MOS1 ₆₅	OS1	0.50	198.5	396.6	899	0.323	0.923	64.7
MOS1 ₇₃ **			225	450		0.367		73.4
MOS1 ₁₀₀			306.4	612.7		0.499		99.9

W: water, C: cement, A: aggregates, S: classical sand, OS1, optimised oyster shell granular skeleton. * Equivalent to MS in Table 6; ** equivalent to MOS1 in Table 6.

Figure 9 presents the compressive strength evolution of the MS_{*i*} and MOS1_{*j*} mortar formulations at 7 days and 28 days with varying cement paste content and varying filling ratios. The classical increase of the compressive strength with curing time was recovered, and the relative increase was still lower for the oyster shell mortar, whatever the filling ratio. This would need further investigation, but it is a confirmation that the oyster shell may slow down the curing process. More interestingly, we can observe that an important increase of the compressive strength was directly linked to an increase in the filling ratio. Traditionally, aggregates are directly replaced in mortar or concrete formulation with no adaptations of the binder content, leading to poor-quality mortar in terms of compressive strength.

Figure 10 illustrates the impact of the filling ratio, which refers to the percentage of voids filled with cement paste, on the compressive strength. This is shown in relation to both the MS and MOS1 formulations, as well as various curing times. Our data indicate that, regardless of the aggregate shape, aggregate material, or curing time, the compressive strength increased as the filling ratio increased, while maintaining a constant aggregate bulk volume. Notably, all of our experimental data appeared to follow a consistent trend, demonstrating the inherent influence of the filling ratio on the material's compressive behaviour at a constant aggregate bulk volume. Given a particular granular skeleton, we can adjust the filling ratio to achieve the optimal balance between the intended compressive strength and the amount of cement paste required. By doing so, we can design cementitious materials that have a lower environmental impact. However, this needs to be further investigated using different values for the filling ratio, as well as different granular distributions and aggregate shapes or materials. The reason behind the trend of increased mortar performance with an increase in cement paste content can be explained by the simple composite mixing rule for oyster shell mortar. In comparison to classical aggregates, oyster shell aggregates are much weaker, and even weaker than the cement paste. Hence, increasing the cement paste content logically results in an increase in the mortar's performance. This trend is usually the opposite for classical concrete, where the aggregates used are stronger than the cement paste. However, in the studies conducted to observe this trend, the cement paste varies along with the fine/coarse aggregate ratio, causing a variation in the aggregate skeleton packing and the aggregate bulk volume as well.

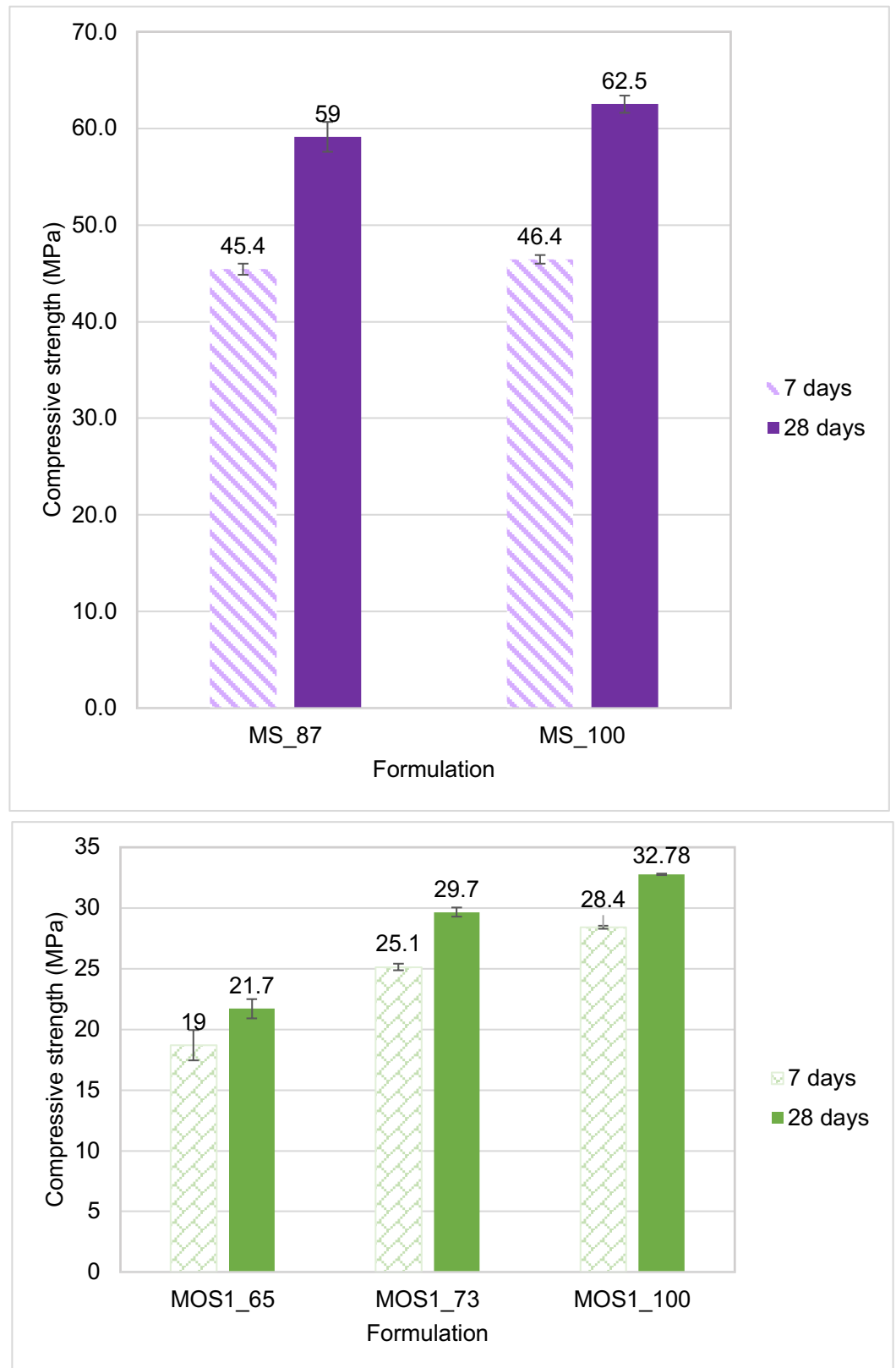


Figure 9. Compressive strength evolution of the MS (top) and MOS1 (bottom) mortar formulations after 7 days (plain) and 28 days (cross-hatch) of curing at varying filling ratios.

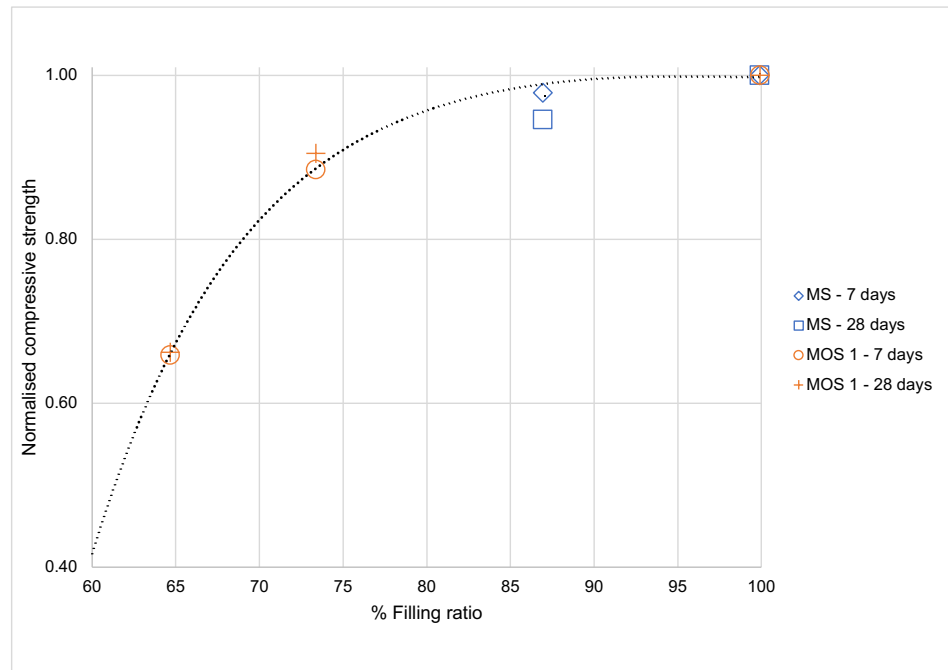


Figure 10. Normalised compressive strength evolution for the MS and MOS1 formulations at different curing times as a function of the filling ratio (the compressive strength is normalised by its value at a 100% filling ratio).

Figure 11 shows the three-point bending flexural strength evolution of the MS_{*i*} and MOS1_{*j*} mortar formulations at 7 days and 28 days with varying cement paste content and varying filling ratios. The previous observation performed under compressive loading still holds: the flexural strength increased with the curing time and the percentage of voids filled with cement paste. However, we can notice that the flexural performances of the mortar made with oyster shell aggregates were close to the ones obtained with the classical sand, whereas the compressive performances observed in Figure 10 were only half of the classical ones. This means that the oyster shell mortar behaves intrinsically better in tension. This also needs to be better investigated, but it may be related to the intrinsic mechanical performances of seashell in tension observed by different authors (e.g., [5–7]).

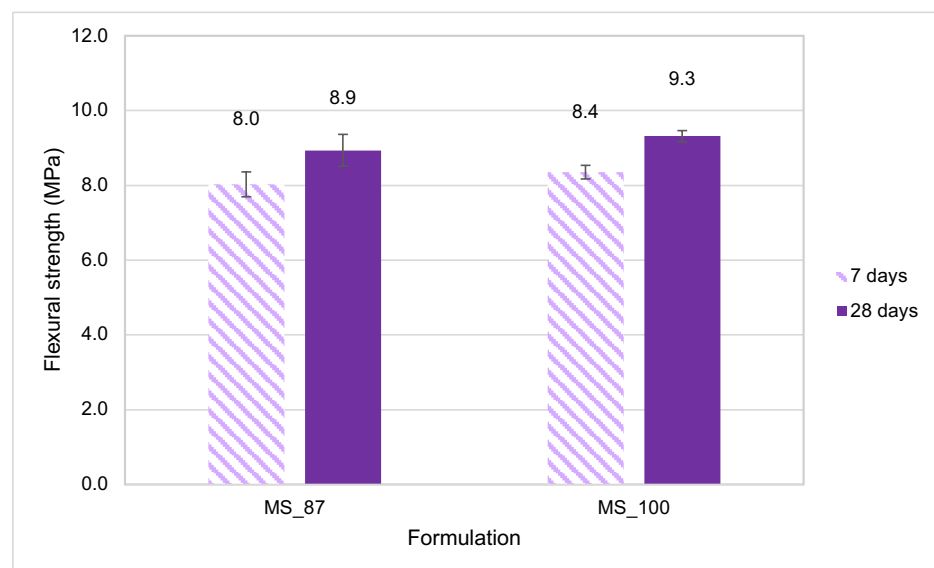


Figure 11. Cont.

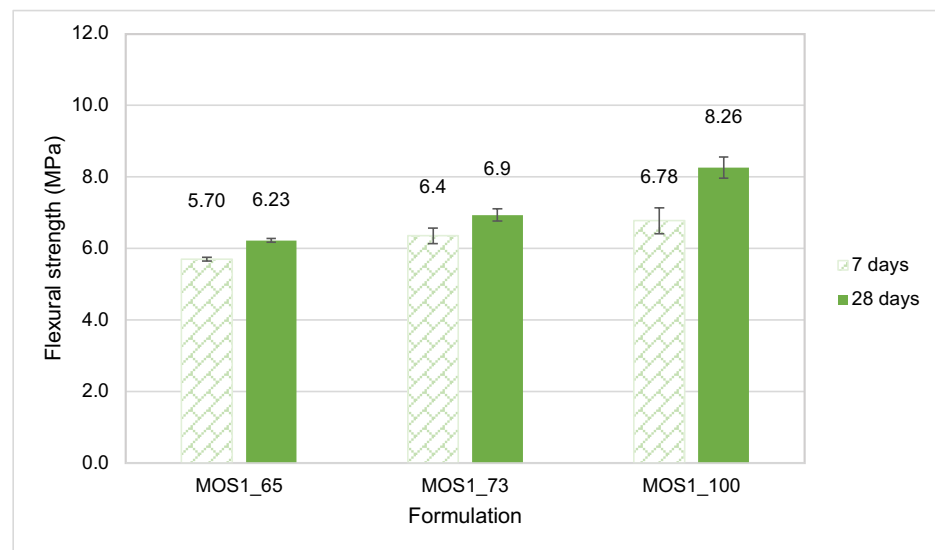


Figure 11. Flexural strength evolution of the MS (top) and MOS1 (bottom) mortar formulations after 7 days (plain) and 28 days (cross-hatch) of curing at varying filling ratios.

4. Concluding Remarks

The following concluding statements can be made:

- A methodology for optimising non-spherical granular skeletons is proposed and validated for oyster shell mortar with complete replacement of aggregates. This method minimises intergranular porosity and enhances the mortar's compressive strength.
- Mimicking a grading curve designed for spherical particles with non-spherical oyster shell aggregates can lead to poor performances in terms of intergranular porosity and compressive strength.
- The high elongation of oyster shell aggregates leads to high intergranular porosities within the skeleton, even after optimisation. Therefore, the cement paste content needs to be adjusted in a 100% oyster shell mortar formulation to improve mechanical performance.
- Increasing the amount of cement paste in a given granular skeleton with a constant aggregate bulk volume leads to an increase in both the filling ratio and mechanical properties, including the compressive and flexural strengths.
- Skeleton optimisation and cement paste content adjustment can restore the good mechanical properties to the oyster shell mortar with a 100% aggregate replacement, particularly in flexural tension.

Author Contributions: Conceptualisation, D.G. and C.P.; methodology, D.G., C.P., O.N. and A.C.P.D.G.; validation, A.C.P.D.G., D.G. and O.N.; formal analysis, A.C.P.D.G. and D.G.; software, A.C.P.D.G.; investigation, A.C.P.D.G. and O.N.; resources, D.G. and C.P.; data curation, D.G. and A.C.P.D.G.; writing—original draft preparation, D.G. and A.C.P.D.G.; writing—review and editing, D.G., A.C.P.D.G. and O.N.; visualisation, A.C.P.D.G. and D.G.; supervision, D.G. and C.P.; project administration, D.G. and C.P.; funding acquisition, D.G., C.P. and O.N. All authors have read and agreed to the published version of the manuscript.

Funding: This work was partially financed by the French *Région Nouvelle Aquitaine* and the French *Comité Régional de la Conchyliculture Arcachon Aquitaine (CRCAA)* through the BECCoH project, by the French *Comité d'Agglomération du Pays Basque* through the Ostra project, by the *Investissement d'Avenir* French programme (ANR-16-IDEX-0002) under the framework of the E2S UPPA hub Newpores, and by the *Institut Universitaire de France*.

Data Availability Statement: The data presented in this study are openly available. Granular skeleton optimisation and influence of the cement paste content in bio-based oyster shell mortar with 100% aggregate replacement [Data set]. Zenodo. Available online: <https://doi.org/10.5281/zenodo.10612803>.

Acknowledgments: The authors gratefully acknowledge Fernando Soares Lameiras for the support provided with the statistical analysis using the software *Minitab 17*[®].

Conflicts of Interest: The authors declare no conflicts of interest.

Abbreviations

The following abbreviations are used in this manuscript:

OS	oyster shell
WA24	water absorption coefficient

References

- Kralj, D.; Markič, M. Building materials reuse and recycle. *WSEAS Trans. Environ. Dev.* **2008**, *4*, 409–418.
- Bardage, S.L. *Performance of Bio-Based Building Materials*; RISE Research Institutes of Sweden: Stockholm, Sweden, 2017.
- Jović, M.; Mandić, M.; Šljivić-Ivanović, M.; Smičiklas, I. Recent trends in application of shell waste from mariculture. *Stud. Mar.* **2019**, *32*, 47–62.
- Summa, D.; Lanzoni, M.; Castaldelli, G.; Fano, E.A.; Tamburini, E. Trends and opportunities of bivalve shells' waste valorization in a prospect of circular blue bioeconomy. *Resources* **2022**, *11*, 48. [[CrossRef](#)]
- Grégoire, D.; Loh, O.Y.; Juster, A.L.; Espinosa, H.D. In-situ AFM Experiments with Discontinuous DIC Applied to Damage Identification in Biomaterials. *Exp. Mech.* **2011**, *51*, 591–607. [[CrossRef](#)]
- Espinosa, H.D.; Juster, A.L.; Latourte, F.J.; Loh, O.Y.; Grégoire, D.; Zavattieri, P.D. Tablet-level origin of toughening in abalone shells and translation to synthetic composite materials. *Nat. Commun.* **2011**, *2*, 173. [[CrossRef](#)]
- Espinosa, H.D.; Grégoire, D.; Latourte, F.; Loh, O. Identification of Deformation Mechanism in Abalone Shells Through AFM and Digital Image Correlation. *Procedia IUTAM* **2012**, *4*, 27–39. [[CrossRef](#)]
- Robert, R.; Sanchez, J.L.; Pérez-Parallé, L.; Ponis, E.; Kamermans, P.; O'Mahoney, M. A glimpse on the mollusc industry in Europe. *Aquac. Eur.* **2013**, *38*, 5–11.
- Bayne, B.; Ahrens, M.; Allen, S.; D'auriac, M.A.; Backeljau, T.; Beninger, P.; Bohn, R.; Boudry, P.; Davis, J.; Green, T.; et al. The proposed dropping of the genus *Crassostrea* for all Pacific cupped oysters and its replacement by a new genus *Magallana*: A dissenting view. *J. Shellfish Res.* **2017**, *36*, 545–547. [[CrossRef](#)]
- Backeljau, T. *Crassostrea gigas* or *Magallana gigas*: A communitybased scientific response. *Biol. Bull.* **2018**, *206*, 46–54.
- H. Silva, T.; Mesquita-Guimarães, J.; Henriques, B.; Silva, F.S.; Fredel, M.C. The potential use of oyster shell waste in new value-added by-product. *Resources* **2019**, *8*, 13. [[CrossRef](#)]
- Ok, Y.S.; Oh, S.E.; Ahmad, M.; Hyun, S.; Kim, K.R.; Moon, D.H.; Lee, S.S.; Lim, K.J.; Jeon, W.T.; Yang, J.E. Effects of natural and calcined oyster shells on Cd and Pb immobilization in contaminated soils. *Environ. Earth Sci.* **2010**, *61*, 1301–1308. [[CrossRef](#)]
- Lee, C.H.; Lee, D.K.; Ali, M.A.; Kim, P.J. Effects of oyster shell on soil chemical and biological properties and cabbage productivity as a liming materials. *Waste Manag.* **2008**, *28*, 2702–2708. [[CrossRef](#)] [[PubMed](#)]
- Lee, S.W.; Kim, Y.M.; Kim, R.H.; Choi, C.S. Nano-structured biogenic calcite: A thermal and chemical approach to folia in oyster shell. *Micron* **2008**, *39*, 380–386. [[CrossRef](#)] [[PubMed](#)]
- Wu, S.C.; Hsu, H.C.; Wu, Y.N.; Ho, W.F. Hydroxyapatite synthesized from oyster shell powders by ball milling and heat treatment. *Mater. Charact.* **2011**, *62*, 1180–1187. [[CrossRef](#)]
- Mo, K.H.; Alengaram, U.J.; Jumaat, M.Z.; Lee, S.C.; Goh, W.I.; Yuen, C.W. Recycling of seashell waste in concrete: A review. *Constr. Build. Mater.* **2018**, *162*, 751–764. [[CrossRef](#)]
- Eziefula, U.G.; Ezech, J.C.; Eziefula, B.I. Properties of seashell aggregate concrete: A review. *Constr. Build. Mater.* **2018**, *192*, 287–300. [[CrossRef](#)]
- Tayeh, B.A.; Hasaniyah, M.W.; Zeyad, A.; Yusuf, M.O. Properties of concrete containing recycled seashells as cement partial replacement: A review. *J. Clean. Prod.* **2019**, *237*, 117723. [[CrossRef](#)]
- Ruslan, H.N.; Muthusamy, K.; Mohsin, S.M.S.; Jose, R.; Omar, R. Oyster shell waste as a concrete ingredient: A review. *Mater. Today Proc.* **2022**, *48*, 713–719. [[CrossRef](#)]
- Hamada, H.M.; Abed, F.; Tayeh, B.; Al Jawahery, M.S.; Majdi, A.; Yousif, S.T. Effect of recycled seashells on concrete properties: A comprehensive review of the recent studies. *Constr. Build. Mater.* **2023**, *376*, 131036. [[CrossRef](#)]
- Yang, E.I.; Yi, S.T.; Leem, Y.M. Effect of oyster shell substituted for fine aggregate on concrete characteristics: Part I. Fundamental properties. *Cem. Concr. Res.* **2005**, *35*, 2175–2182. [[CrossRef](#)]
- Yang, E.I.; Kim, M.Y.; Park, H.G.; Yi, S.T. Effect of partial replacement of sand with dry oyster shell on the long-term performance of concrete. *Constr. Build. Mater.* **2010**, *24*, 758–765. [[CrossRef](#)]
- Eo, S.H.; Yi, S.T. Effect of oyster shell as an aggregate replacement on the characteristics of concrete. *Mag. Concr. Res.* **2015**, *67*, 833–842. [[CrossRef](#)]
- Kuo, W.T.; Wang, H.Y.; Shu, C.Y.; Su, D.S. Engineering properties of controlled low-strength materials containing waste oyster shells. *Constr. Build. Mater.* **2013**, *46*, 128–133. [[CrossRef](#)]

25. Wang, H.Y.; Kuo, W.T.; Lin, C.C.; Po-Yo, C. Study of the material properties of fly ash added to oyster cement mortar. *Constr. Build. Mater.* **2013**, *41*, 532–537. [[CrossRef](#)]
26. Liao, Y.; Wang, X.; Kong, D.; Da, B.; Chen, D. Experiment research on effect of oyster shell particle size on mortar transmission properties. *Constr. Build. Mater.* **2023**, *375*, 131012. [[CrossRef](#)]
27. Bamigboye, G.O.; Okechukwu, U.E.; Olukanni, D.O.; Basse, D.E.; Okorie, U.E.; Adebesein, J.; Jolayemi, K.J. Effective Economic Combination of Waste Seashell and River Sand as Fine Aggregate in Green Concrete. *Sustainability* **2022**, *14*, 12822. [[CrossRef](#)]
28. Kim, Y.Y.; Lee, K.M.; Bang, J.W.; Kwon, S.J. Effect of W/C ratio on durability and porosity in cement mortar with constant cement amount. *Adv. Mater. Sci. Eng.* **2014**, *2014*. [[CrossRef](#)]
29. Lian, C.; Zhuge, Y.; Beecham, S. The relationship between porosity and strength for porous concrete. *Constr. Build. Mater.* **2011**, *25*, 4294–4298. [[CrossRef](#)]
30. Fennis, S.A.; Walraven, J.C.; Den Uijl, J.A. The use of particle packing models to design ecological concrete. *Heron* **2009**, *54*, 183–202.
31. Kumar, S.V.; Santhanam, M. Particle packing theories and their application in concrete mixture proportioning: A review. *Indian Concr. J.* **2003**, *77*, 1324–1331.
32. Fuller, W.; Thompson, S. The laws of proportioning concrete. *ASCE J. Transp.* **1907**, *59*, 67–143. [[CrossRef](#)]
33. Andersen, P.; Johansen, V. Particle packing and concrete properties. *Mater. Sci. Concr.* **1991**, *II*, 111–147.
34. Mehdipour, I.; Khayat, K.H. Understanding the role of particle packing characteristics in rheo-physical properties of cementitious suspensions: A literature review. *Constr. Build. Mater.* **2018**, *161*, 340–353. [[CrossRef](#)]
35. De Larrard, F. *Structures Granulaires et Formulation Des Bétons*; Laboratoire central des ponts et chaussées: Paris, France, 2000.
36. de Larrard, F. *Concrete Mixture Proportioning: A Scientific Approach*; E and FN Spon: London, UK, 1999.
37. Goltermann, P.; Johansen, V.; Palbol, L. Packing Aggregates: An Alternative Tool to Determine the Optimal Aggregate Mix. *ACI Mater. J.* **1997**, *94*, 435–443.
38. Yu, A.B.; Standish, N.; Mclean, A. Porosity calculation of binary mixtures of nonspherical particles. *J. Am. Ceram. Soc.* **1993**, *76*, 2813–2816. [[CrossRef](#)]
39. Yu, A.B.; Standish, N. Characterisation of non-spherical particles from their packing behaviour. *Powder Technol.* **1993**, *74*, 205–213. [[CrossRef](#)]
40. AFNOR. *NF EN 1097; Test For Mechanical and Physical Properties of Aggregates—Part 6: Determination of Particle Density and Water Absorption*. European Standard; Association Française de Normalisation: Saint Denis, France, 2014.
41. AFNOR. *NF EN 1097; Test for Mechanical and Physical Properties of Aggregates—Part 3: Determination of Loose Bulk Density and Voids*. European Standard; Association Française de Normalisation: Saint Denis, France, 1998.
42. AFNOR. *NF EN 933; Tests for Geometrical Properties of Aggregates—Part 1: Determination of Particle Size Distribution—Sieving Method*. European Standard; Association Française de Normalisation: Saint Denis, France, 2012.
43. AFNOR. *NF EN 933; Tests for Geometrical Properties of Aggregates—Part 3: Determination of Particle Shape—Flakiness Index*. European Standard; Association Française de Normalisation: Saint Denis, France, 2012.
44. AFNOR. *NF EN 933; Tests for Geometrical Properties of Aggregates—Part 4: Determination of Particle Shape—Shape Index*. European Standard; Association Française de Normalisation: Saint Denis, France, 2008.
45. AFNOR. *NF EN 196; Methods for Testing Cement—Part 1: Determination of Strength*. European Standard; Association Française De Normalisation: Saint Denis, France, 2016.
46. AFNOR. *NF EN 1015; Methods of Test for Mortar for Masonry—Part 11 : Determination of Flexural and Compressive Strength of Hardened Mortar*. European Standard; Association Française de Normalisation: Saint Denis, France, 2019.
47. Safi, B.; Saidi, M.; Daoui, A.; Bellal, A.; Mechekak, A.; Toumi, K. The use of seashells as a fine aggregate (by sand substitution) in self-compacting mortar (SCM). *Constr. Build. Mater.* **2015**, *78*, 430–438. [[CrossRef](#)]

Disclaimer/Publisher’s Note: The statements, opinions and data contained in all publications are solely those of the individual author(s) and contributor(s) and not of MDPI and/or the editor(s). MDPI and/or the editor(s) disclaim responsibility for any injury to people or property resulting from any ideas, methods, instructions or products referred to in the content.